

Reactive scattering of $F+HD\rightarrow HF(v,J)+D$: $HF(v,J)$ nascent product state distributions and evidence for quantum transition state resonances

Warren W. Harper,^{a)} Sergey A. Nizkorodov,^{b)} and David J. Nesbitt

JILA, National Institute of Standards and Technology and University of Colorado and Department of Chemistry and Biochemistry, University of Colorado, Boulder, Colorado 80309-0440

(Received 31 October 2001; accepted 11 January 2002)

Single collision reactive scattering dynamics of $F+HD\rightarrow HF(v,J)+D$ have been investigated exploiting high-resolution ($\Delta\nu\approx 0.0001\text{ cm}^{-1}$) infrared laser absorption for quantum state resolved detection of nascent $HF(v,J)$ product states. State resolved Doppler profiles are recorded for a series of HF rovibrational transitions and converted into state resolved fluxes via density-to-flux analysis, yielding cross-section data for relative formation of $HF(v,J)$ at $E_{\text{com}}\approx 0.6(2)$, $1.0(3)$, $1.5(3)$, and $1.9(4)$ kcal/mol. State resolved $HF(v,J)$ products at all but the lowest collision energy exhibit Boltzmann-type populations, characteristic of *direct reactive scattering* dynamics. At the lowest collision energy [$E_{\text{com}}\approx 0.6(2)$ kcal/mol], however, the $HF(v=2,J)$ populations behave quite anomalously, exhibiting a nearly “flat” distribution out to $J\approx 11$ before dropping rapidly to zero at the energetic limit. These results provide strong experimental support for quantum transition state resonance dynamics near $E_{\text{com}}\approx 0.6$ kcal/mol corresponding classically to H atom chattering between the F and D atoms, and prove to be in remarkably quantitative agreement with theoretical wave packet predictions by Skodje *et al.* [J. Chem. Phys. **112**, 4536 (2000)]. These fully quantum state resolved studies therefore nicely complement the recent crossed beam studies of Dong *et al.* [J. Chem. Phys. **113**, 3633 (2000)], which confirm the presence of this resonance via angle resolved differential cross-section measurements. The observed quantum state distributions near threshold also indicate several rotational states in the $HF(v=3)$ vibrational manifold energetically inaccessible to $F(^2P_{3/2})$ reagent, but which are consistent with a minor ($\leq 5\%$) nonadiabatic contribution from spin-orbit excited $F^*(^2P_{1/2})$. © 2002 American Institute of Physics. [DOI: 10.1063/1.1456507]

I. INTRODUCTION

The $F+H_2\rightarrow HF(v,J)+H$ reaction has been of enormous fundamental importance in the study of chemical reaction dynamics. This system with its $F+HD$, $F+D_2$ isotopic variants represent the simplest exothermic three-atom bimolecular reaction and has been subjected to increasing levels of scrutiny from both experimental^{1–8} and theoretical^{9–13} perspectives. This class of H atom abstraction reaction has been experimentally investigated using methods ranging from the classic arrested relaxation infrared (IR) chemiluminescence studies of Polanyi and co-workers,^{14,15} to crossed beam detection of HF/DF products via moderate resolution energy loss methods,^{7,8} to recent high resolution crossed beam studies via Rydberg tagging and time of flight analysis of H/D atom recoil.^{16,17} Full three-dimensional (3D) quantum theoretical studies of these reactions are tractable due to the presence of only a single heavy (i.e., nonhydrogenic) atom. Indeed, the $F+H_2$ system represents one of the few reactions that have successfully permitted study in full dimensionality at the *ab initio* level, with converged calculations feasible without any dynamical approximations other

than Born–Oppenheimer propagation on a single adiabatic potential surface. This confluence of fully quantum state resolved experiment and theory has provided a powerful opportunity for testing potential surfaces and dynamical methods as well as the requisite “intellectual fuel” for numerous controversies over the years.

Although the isotopically related $F+HD$ system shares the same Born–Oppenheimer (i.e., adiabatic) potential energy surface with $F+H_2$, there are subtle but important differences that have made it of compelling dynamical interest. First of all, the H_2 symmetry is broken by a D atom substitution, which makes reactive events at the two ends of the molecule experimentally distinguishable. Thus, in the limit of *direct* reactive scattering dynamics, one can isolate dynamical pathways semiclassically corresponding to F atom attack on D or H end by detection of HF or DF product. Second, this asymmetry eliminates the role of ortho/para nuclear spin states in reagent HD, which therefore permits efficient cooling in the supersonic expansion environment into nearly a single ($J\approx 0$) rotational level. Of primary dynamical importance for this work, however, is that D atom substitution provides a F–H–D “heavy+light-heavy” transition state for F attack on the H atom, which has been predicted¹⁸ to enhance quantum “transition state resonances” corresponding to excitation of quasibound vibrational motion weakly coupled to the reaction coordinate. Indeed, the role of

^{a)}Current address: Pacific Northwest National Laboratory, P.O. Box 999 MS K5-25, Richland, WA 99352.

^{b)}Current address: California Institute of Technology, M/C 127-72, Pasadena, CA 91125.

such transition state resonances in the $F+H_2$ reaction system has been one of long standing controversy, for which a full consensus is still not yet achieved. However, there is now strong theoretical evidence^{18,19} for a broad quantum transition state resonance in $F+HD$ at low collision energies (≈ 0.5 kcal/mol), corresponding semiclassically to rapid H atom “chattering” between the heavier F and D atom. Experimental confirmation of such transition state resonance dynamics has been elegantly provided in the Liu laboratory^{18,19} by time-of-flight analysis of the D atom product, specifically monitoring angular changes in the vibrationally resolved differential cross sections as a function of collision energy.

As a special motivating force for the current studies, an anomalous and distinctive independent signature of this quantum transition state resonance is also predicted in the $HF(v,J)$ rotational state distributions. Wave packet calculations by the Skodje group^{18,20} predict two qualitatively different classes of product state distributions for $HF(v,J)$ products. Far away from the resonance energy, product formation is predicted to occur by “direct” reactive scattering, yielding distributions with a gradual, “Boltzmann-like” dropoff in rotational J state. Products from the transition state resonance channel, on the other hand, are thought to occur via tunneling through a strongly noncollinear barrier, which is therefore greatly enhanced by rotational excitation of the nascent HF in the transition state region. As a result of this competition between (i) J dependent enhancement of resonance decay rate and (ii) J dependent drop off due to energetic constraints, the $HF(v,J)$ product states have been predicted²⁰ to yield nearly “flat” J distributions (although with significantly local structure) right up to the energetic cutoff. Such tests for the rotational “signatures” of quantum transition-state resonance behavior requires complete experimental resolution of the nascent $HF(v,J)$ rotational state populations as a function of collision energy, which represents the primary thrust of this paper.

To achieve the necessary quantum state detection specificity, we have combined high sensitivity, single-mode IR laser absorption methods with crossed beam reactive scattering for direct monitoring of nascent products under rigorously single collision conditions. The crucial advantage of single mode sources for studying reaction dynamics is the high spectral resolution ($\Delta\nu\approx 0.0001\text{ cm}^{-1}$), which translates into $HF(v,J)$ product state detection with complete rovibrational quantum state resolution. In fact, the intrinsic velocity resolution is sufficiently good (\approx few meters/s) that the absorption profiles exhibit Doppler line broadening effects due to HF translational energy recoil, the dynamics of which can be studied for favorable kinematic mass combinations by high resolution IR laser Dopplerimetry methods. This has been most recently demonstrated for $F+CH_4$ reactive scattering,^{21,22} for which the CH_3 product provides a sufficient mass for developing substantially high HF recoil speeds in the reactive event. This capability permits detection and elucidation of frequency dependent Doppler profiles from (i) stimulated emission (near line center) and (ii) absorption (at large detuning) due to velocity dependent population inversions in the crossed jet reaction zone. These in-

versions can be readily rationalized by conservation of energy in the reactive event, with the more internally energetic upper states having less energy left for velocity recoil. Although high resolution Dopplerimetry on $F+HD$ is substantially more difficult by virtue of smaller reduced mass for the ejecting D atom, it represents a twofold improvement over $F+H_2$ kinematics and can indeed be partially resolved. Most importantly, however, studies with complete resolution of rovibrational quantum states provide a rare opportunity for rigorous benchmark comparisons between experiment and theory for fundamental atom+diatom reaction dynamics on a single, well characterized potential energy surface.

The organization of the rest of this paper is as follows. Section II briefly summarizes the experimental method with emphasis on details relevant to the present study. Section III follows with Doppler resolved absorption results on $F+HD$ reactive scattering, followed in Sec. IV by Monte Carlo simulations of the density-to-flux transformation, which are necessary to obtain nascent $HF(v,J)$ product state distributions from direct absorption measurements as a function of center-of-mass collision energy. Comparison of the experimental $HF(v,J)$ product state distributions with *ab initio* theoretical dynamics calculations by Chao *et al.* are discussed in Sec. V, with particular focus on anomalous changes in the $HF(v=2,J)$ distribution topology at collision energies near the predicted transition state resonance. Furthermore, analysis of the near threshold $HF(v=3,J)$ product distributions at $E_{\text{com}}=0.6(2)$ kcal/mol indicate weak branching into rotational levels energetically inaccessible to ground state $F(^2P_{3/2})+HD$ reactions, suggesting the presence of minor ($\leq 5\%$) contributions from nonadiabatic $F^*(^2P_{1/2})+HD$ channels. Section VI summarizes and concludes the paper.

II. EXPERIMENT

The crossed jet apparatus has been described in detail previously;^{1,2,21} only features pertinent to the current study will be briefly summarized in this section. The reaction vessel is a 65 L vacuum chamber pumped by a 10 in. diffusion pump fitted with a water-cooled baffle trap and roughed with a Roots²³ blower. Two pulsed valves oriented at right angles to the probe laser deliver short gas pulses of jet cooled F and HD reagents, at total densities such that the collision probability is $< 1\%$; thus the probability of reagents/products experiencing multiple collisions can be safely neglected. The chamber is pumped out to a background pressure of $< 5 \times 10^{-6}$ Torr and remains below 1×10^{-4} Torr with both valves running at 10 Hz. After the reaction event, the HF product is detected by high-resolution IR laser absorption monitored using two matched InSb detectors to record the transient absorbance response for each HF rovibrational transition of interest. Figure 1 provides a schematic of the experimental setup, where the two jet expansion axes are mutually orthogonal to each other and the detection laser. The contours drawn in the jet intersection region (obtained from detailed Monte Carlo simulations described in Sec. IV A) illustrate the probability of detecting HF after a reactive event. These contours are very strongly peaked within a small detection volume ($\approx 3\text{ cm}^3$) at the jet intersection region, with low probability tails that extend toward each

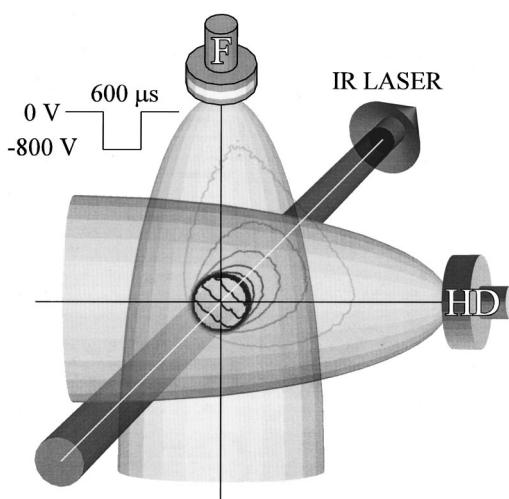


FIG. 1. Schematic of the crossed supersonic jet experiment for F+HD reaction dynamics. Nascent HF(v,J) product states are formed and detected via shot noise limited direct absorption with a single mode IR laser multipassed 20 times through the jet intersection region in a Herriot cell configuration. The set of contours (in 10% increments) represent Monte Carlo simulations of events producing HF from a specific spot in the jet intersection region (see text for details). The contours are strongly peaked in the detection volume, but extending slightly toward each valve.

pulsed valve. These tails are due to single collision F+HD reactions occurring slightly upstream, yielding products recoiling collision free into the laser detection region. This necessarily translates into a distribution of collision geometries and thus a somewhat broader range of collision energies than could be obtained with skimmed beams. However, the implementation of crossed jets as opposed to skimmed beams is dictated by sensitivity demands for long absorption path lengths, which provide necessary detection limits for absorbers such as HF down to $<10^7$ molecules/cm³/quantum state.

The reactive F atoms are produced *in situ* for each pulse by passing a 5% fluorine/95% argon mixture through a pulsed discharge valve located 5.1 cm from the intersection region. The F-atom source consists of two electrodes mounted at the exit of a solenoid valve, one of which is in contact with the metal body of the valve. As the gas pulse (≈ 1 ms duration) expands into the vacuum, a high voltage pulse (≈ -800 V, $600 \mu\text{s}$) is applied to the bottom of two electrodes separated by a thin ($550 \mu\text{m}$) Kel-F spacer. The resulting current pulse first crosses a 500Ω ballast resistor before going to the electrode, stabilizing the discharge and allowing a convenient measurement of real time currents (≈ 0.4 – 0.5 A peak). The limiting orifice of the valve is a $500 \mu\text{m} \times 5$ mm slit, optimized to provide stable discharges on the week-long time scale between routine maintenance. As a consequence of the slit valve, the angular distributions are functions of both θ (angle from expansion axis) and ϕ (angle about the expansion axis). However, these can be measured directly by doping a small amount of HF or CH₄ into the 5% fluorine/argon mixture, recording Doppler absorbances, and inverting these profiles analytically to obtain angular distributions. The angular distributions for each ϕ can be well characterized as power laws in $\cos^n(\theta)$, with half width at

half maximum (HWHM) values of 19° and 40° for the limiting cases parallel and perpendicular to the slit axis. Reactive scattering experiments are performed with the slit parallel to the laser axis (perpendicular to the HD expansion); this configuration has the advantage of prefocusing the initial F atom reagent (and thus HF absorption signals) into a narrower Doppler velocity group without loss of absorption path length. The F₂/Ar jet speed can be obtained either by direct laser Dopplerimetry or time-of-flight of absorption signals;¹ the measured value of $560(5)$ m/s agrees well with calculated speeds from standard adiabatic expansion formulas.

The HD source consists of HD/argon gas mixtures expanding through a piezoelectric valve²⁴ with a $145(5) \mu\text{m}$ orifice and $200 \mu\text{s}$ gas pulse, timed to coincide with the F atom source in the intersection region. The reagent HD jet is characterized by recording Doppler profiles for small dopant levels of HF or CH₄ in the argon/HD gas mixtures and inverting to angular distributions for each gas mixture. On-axis jet speeds are measured using Dopplerimetry or optical time-of-flight techniques,¹ yielding $2310(25)$ m/s (neat HD), $1970(30)$ m/s (3% Ar/HD), $1620(40)$ m/s (9% Ar/HD), and $1150(40)$ m/s (25% Ar/HD) as a function of expansion dilution.

Of special importance is the distribution of rotational states in the HD jet. In the previous studies of F+H₂ dynamics, complete cooling of the H₂(J) reagent distributions was limited by $\Delta J=2$ partially rotational energy differences and lack of ortho/para spin relaxation channels. This absence of full rotational relaxation for H₂ expansions could be inferred from the measured terminal jet speeds, which were *slower* than predicted from adiabatic heat capacity formulas due to unrelaxed H₂ rotational energy.¹ From a similar analysis of terminal jet speeds for neat HD expansions, the rotational temperature can be estimated to be ≤ 50 K, which would predict HD populations of 0.812:0.186:0.002 for HD($J=0,1,2$), i.e., largely confined to the ground state. In fact, this HD rotational cooling improves dramatically with Ar diluent, where reverse seeding is utilized to slow down the HD reagent for the lowest collision energies sampled. Under these Ar diluent conditions, we conservatively estimate the HD rotational temperature to be ≤ 40 K, which translates into upper limit HD($J=0,1,2$) populations of 0.892:0.107: <0.001 , respectively. This proves to be relevant for studies of the transition state resonance dynamics at the lowest collision energies sampled ($E_{\text{com}} \approx 0.6$ kcal/mol), which therefore take place with nearly pure HD($J=0$) reagent and only $\leq 11\%$ contributions from any rotationally excited HD($J \geq 1$).

The HD gas is prepared using the exothermic reaction $\text{LiD}(s) + \text{H}_2\text{O}(l) \rightarrow \text{HD}(g) + \text{LiOH}(s)$, which goes to completion even at high HD gas pressures. A vacuum tight reactor is fabricated from a stainless steel pipe with flanges welded on each end and gas line connections attached to one end. LiD(s) reagent is placed in a stainless steel cage that can be lowered in the reactor under vacuum into excess deionized H₂O. The reactor is assembled and evacuated down to the vapor pressure of water in order to remove residual nitrogen and oxygen. The cage is then slowly lowered

into the water to trigger a vigorous chemical reaction (cooled with an alcohol bath of -10°C), which can be conveniently moderated by regulating cage height. The resulting HD product is collected in a gas cylinder after passing through a -100°C silica bead trap to remove residual water vapor; HD pressures of 300 psi can be easily obtained and controlled by the amount of LiD reagent. The HD synthesis method is limited by LiD isotopic purity to $\approx 99\%$, as directly quantified by rotationally resolved Raman spectroscopy on sample gas aliquots. During experimental runs, a cold trap (-80°C) removes any trace residual H_2O vapor present in the HD just prior to the pulsed valve.

The infrared laser has been described previously.^{1,21,25} The cw IR source is a Kr^+ pumped color center laser, retrofitted with tunable intracavity galvo plates and an etalon servoloop for continuous, single mode scanning. The IR is split into two equal signal and reference beams, with the signal beam going through the vacuum chamber in a Herriott cell^{26,27} multipass configuration (20 passes) to enhance detection sensitivity. Signal and reference photocurrents are subtracted down to the shot noise limit using servoloop electronics with 10^5 -fold common mode rejection. The difference signal is low pass filtered, recorded with a transient digitizer, and transferred to a computer for analysis and data storage. Software integration is used to isolate transient signal changes occurring in the temporal overlap between the two crossed jets, with DC IR power levels monitored to yield absolute absorbances. IR power levels are $<100\ \mu\text{W}$ to ensure negligible perturbation of rovibrational populations by stimulated absorption/emission effects as well as maintain detectors in a linear regime. Minimum detectable absorbance (in a nominal 20 kHz detection bandwidth) is $\approx 1 \times 10^{-5}$, translating into a sensitivity of 5×10^6 HF(*v*,*J*) products/ $\text{cm}^3/\text{quantum state}$ with modest signal averaging.

III. RESULTS

High-resolution Doppler profiles of HF(*v*,*J*) product have been recorded over all relevant HF $\Delta v = \pm 1$ transitions within the tuning range of the color center IR laser (2.5–3.3 μm), and at each of four collision energies [$E_{\text{com}} \approx 0.6(2)$, 1.0(3), 1.5(3), and 1.9(4) kcal/mol]. Particular attention has naturally been focused on transitions out of the $v''=2$ and $v''=3$ manifold, where quantum transition-state resonance and near threshold effects are predicted to be most relevant. Transitions originating from the HF($v''=1, J$) manifold have also been studied at the two highest collision energies, but this proves unfeasible at current signal-to-noise levels due to rapid decrease in signal intensity for collision energies below the activation barrier. Scans are performed over $\geq 0.1\ \text{cm}^{-1}$ around the transition center, which for typical profiles correspond to a 10-fold broader baseline than the Doppler FWHM. Signal scans are corrected for weak background absorptions due to trace HF impurities in the F atom discharge source ($<10\%$ of peak signals) by repeating the scans with the HD valve on and off. Figure 2 shows representative R-branch data at $E_{\text{com}} = 1.9\ \text{kcal/mol}$ collision energy, revealing “strong” absorbance signals of $\approx 2 \times 10^{-4}$ with the rms shot noise limited noise of $\approx 2 \times 10^{-5}$ and signal to noise (S/N) ≈ 10 . Also shown are profiles obtained from a

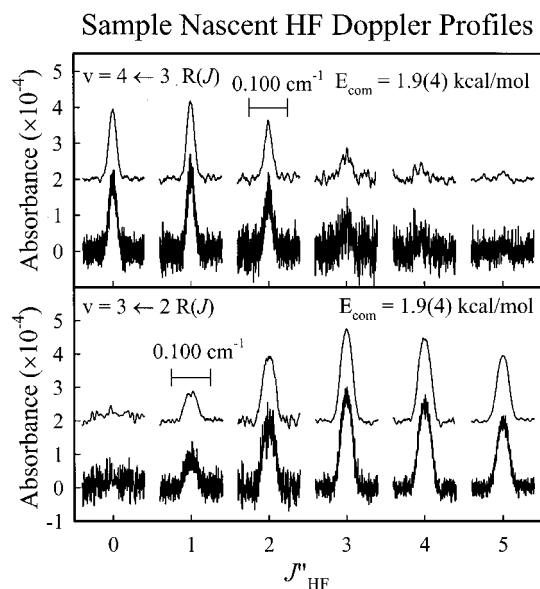


FIG. 2. Sample Doppler profile data on nascent HF(*v*,*J*) product states from F+HD reactive events.

Savitzky–Golay filtering process,²⁸ which takes advantage of the large number of laser frequency steps sampled over the full scanning event. Additional S/N enhancement in the overall data set is achieved by (i) scanning each transition multiple times, (ii) probing redundant transitions out of the same state, as well as (iii) integrating over Doppler profiles to obtain column integrated densities. Reference data on the $v=3 \leftarrow 2$; $R(4)$ transition is recorded for normalization at regular intervals during all experimental runs; this successfully corrects for low frequency drift and day-to-day fluctuations in F-atom production efficiency. As an indication of intentional redundancy in data acquisition, the total number of Doppler scan measurements and quantum state populations determined are summarized in Table I for each collision energy. In all cases, there are fourfold to sixfold more measurements than the number of quantum states populated, which is sufficiently over-determined to permit high S/N extraction of populations.

The high resolution Doppler absorbance profiles, $A(\nu)$, are integrated over the laser frequency and converted to quantum state resolved column-integrated densities (CID) according to

$$\int A(\nu) d\nu = \frac{8\pi^3 \nu_0 |m| \mu^2}{3hc} \left[\frac{\int [\text{HF}(v'', J'')] dl}{(2J''+1)} - \frac{\int [\text{HF}(v', J')] dl}{(2J'+1)} \right], \quad (1)$$

where ν_0 is the transition center frequency, $m=J''+1$ ($-J''$) for $R(P)$ branch transitions, and μ represents the transition dipole moment obtained from extensive studies by Setser²⁹ and Stwalley.³⁰ Equation (1) has been used to least squares fit the entire set of absorption data for each of the four collision energies, yielding column-integrated densities as a function of final HF(*v*,*J*) product state. Due to the large number of redundant measurements for each J state, the

TABLE I. Summary of probed HF(v, J) levels for each collision energy. Numbers reflect the total of all repetitive measurements, with the values in parentheses indicating the number of unique transitions [i.e., $v' \leftarrow v''$, $R(J)$] probed.

Collision energy (kcal/mol)	Total number of transitions	<i>P</i> -branch transitions	<i>R</i> -branch transitions	v, J populations determined	Number of reference lines
1.9(4)	176(72)	96 (40)	80 (32)	40	86
1.5(3)	159(59)	69 (29)	90 (30)	39	66
1.0(3)	147(40)	60 (18)	87 (22)	24	66
0.6(2)	98(30)	20 (10)	78 (20)	20	42

variance–covariance matrix resulting from the least squares fit describes the uncertainties in these column-integrated densities reasonably well.

IV. ANALYSIS

The primary data from these experimental studies are column-integrated *densities* of nascent HF(v, J) product. However, the more fundamental quantity characterizing reaction dynamics is the reactive *flux* into a specific quantum state, which therefore requires a careful consideration of the density-to-flux transformation. For direct absorption measurements, this transformation requires scaling integrated absorbance signals by the residence time in the laser beam for a given HF(v, J) product state. Since the center-of-mass velocity vector is largely carried by the F atom motion, these density to flux scaling factors can be estimated from detailed Monte Carlo simulations for a given experimental geometry, with only modest theoretical input on angular scattering distributions, as described below. Indeed, these simulations also permit many other useful statistics for the collision ensemble to be obtained, such as the mean and spread in the distribution of sampled collision energies (E_{com}). Finally, the experimentally inferred fluxes of HF(v, J) product states can be translated into the desired relative cross sections from known reagent densities and the average relative velocity, $\langle v_{\text{rel}} \rangle$.

A. Monte Carlo simulations

As mentioned above, to achieve suitable signal/noise levels with shot noise limited IR laser absorbance methods, the current experiments take advantage of unskimmed supersonic jets to provide significantly enhanced path lengths (≈ 50 cm) while still maintaining single collision conditions. This necessarily introduces a range of angles with which the reagent species collide; even for supersonically cooled expansions this leads to a finite distribution of collision energies, $P(E_{\text{com}})$. To obtain these distributions, we have utilized Monte Carlo simulations, the details of which have been described in previous work on the F+CH₄ reaction system.^{21,22} As input data, high resolution IR laser Dopplerimetry techniques are first used to measure the jet angular distributions, while jet speeds along the expansion axis are characterized using optical time-of-flight methods. To estimate the resulting spread in collision energies, points are randomly selected in the experimental detection region, which is conservatively approximated as a cube with the pulsed valves centered on adjacent faces. The center-of-mass collision energy is then

calculated from known speeds and collision geometries, appropriately weighted by relative velocity vectors and reagent densities, i.e., $\propto \rho_1 \rho_2 |v_{\text{rel}}|$. Monte Carlo integration is performed by randomly sampling over a sufficiently large number of points ($\approx 10^8$) inside the detection volume to ensure convergence. Collision energy distributions for the four experimental conditions are shown in Figs. 3 and 4, with the first and second central moments denoted by vertical and horizontal lines, respectively. As expected, the collision energy uncertainties are dominated by the distribution of collision geometries and impacted to a much weaker extent by the much narrower distribution of supersonic jet speeds. For

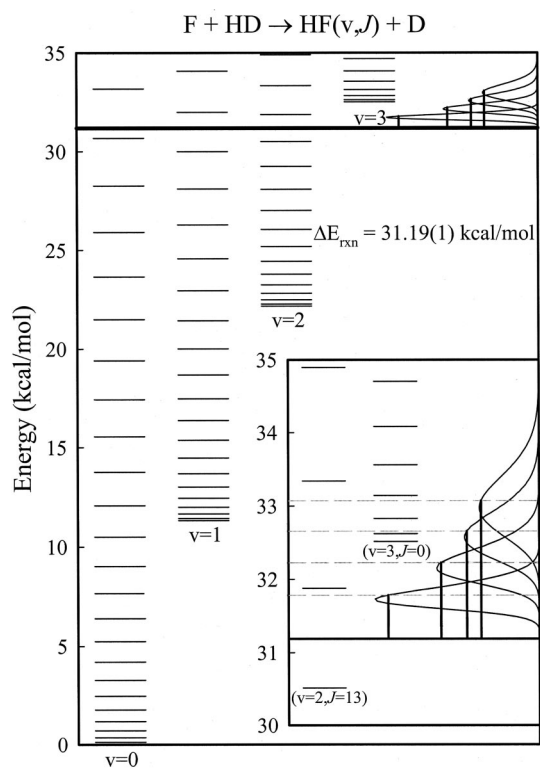


FIG. 3. Energetics for the F+HD reaction. The heavy solid line indicates the 31.19(1) kcal/mol reaction exothermicity, while the curves in the upper right corner represent the additional center of mass collision energy (see also Fig. 4). All HF(v, J) product states below a given collision energy distribution are energetically accessible. The blow up of this region (see inset) displays the threshold levels along with the energy available for each collision energy.

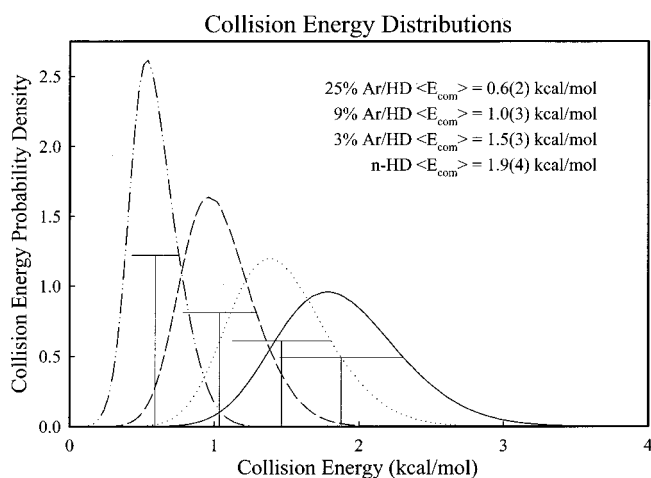


FIG. 4. Monte Carlo calculated collision energy distributions for each collision energy studied in this work. Note that the distributions are near Gaussian, with a slight asymmetry extending to higher collision energies. The vertical and horizontal lines indicate average and variance for each distribution.

a simple rule of thumb, the FWHM values scale more or less linearly in $\langle E_{\text{com}} \rangle$, corresponding to a roughly 25% spread in collision energies. (See Table II.)

To correctly determine final state fluxes (j) from column integrated densities (ρ) requires a density-to-flux transformation. The experimentally determined averages of these quantities are linked by $\langle \rho \rangle = \langle j/v_{\perp} \rangle$, where v_{\perp} is the laboratory frame recoil velocity component perpendicular to the laser probe axis. The average reciprocal speed $\langle 1/v_{\perp} \rangle$ scales as the average residence time $\langle \tau \rangle$ in the laser beam; thus the density-to-flux transformation is simply proportional to $1/\langle \tau \rangle$; note that this differs from $\langle 1/\tau \rangle$ for any finite spread in τ . One advantage of the F+HD system is that the reaction exothermicity is known from spectroscopic measurements of HF and HD bond strengths to ≈ 0.01 kcal/mol accuracy.^{31,32} Thus the recoil speed of any HF(v, J) product state can be reliably obtained from conservation of energy and momentum for a known incident collision energy and reaction exothermicity. For a discretized bin of scattering angles in the center-of-mass frame, the average residence time $\langle \tau \rangle$ can therefore be explicitly calculated. This also permits us to construct predicted laboratory frame Doppler profiles for scattering into a given center-of-mass angular range, which represents the first step in a high resolution Dopplerimetry analysis.

For light H or D atom ejection, however, the recoil speeds imparted to the product HF(v, J) are only comparable to the initial velocity spread in the jet. Though these recoil distributions clearly impact the data via line broadening, the

effects are insufficiently dominant to make a full Dopplerimetry analysis feasible. As a compromise, therefore, the density-to-flux multipliers (DFM) are constructed from a weighted sum:

$$\text{DFM}(v, J) = \left[\sum_{i=\cos(\theta_i)}^{i=\cos(\pi)} \langle \tau_{i,v,J} \rangle \times W_{i,v,J} \right]^{-1}, \quad (2)$$

where (i) $\langle \tau_{i,v,J} \rangle$ are the average residence times calculated for each HF(v, J) quantum state in a specific $\cos(\theta_i)$ bin, and (ii) $w_{i,v,J}$ are normalized weights proportional to theoretically²⁰ calculated differential cross sections. While this density-to-flux transformation relies on theoretical input, this dependence is not overly strong since the residence time τ is largely dominated by forward center of mass motion in the laboratory frame. As shown in Eq. (2), the density-to-flux multiplier is equal to the inverse of the differential-cross-section averaged residence time, so that the density-to-flux transformation is achieved simply by multiplying by DFM(v, J). The resulting fluxes have also been scaled by argon dilution in the HD jet as well as by average collision speed ($|v_{\text{rel}}|$) to obtain results directly proportional to the desired state-to-state reaction cross sections.

B. Nascent HF(v, J) populations and relative state-to-state cross sections

Table III reports relative cross sections for formation of HF(v, J) product states at each of the four collision energies studied. The full data set has been normalized to 100% only for the highest collision energy [$E_{\text{com}} = 1.9(4)$ kcal/mol], so the v, J dependent changes in state-to-state cross sections with decreasing collision energy are accurately reflected. The DFM(v, J) values used in the density to cross-section transformation differ by approximately equal twofold over all vibrational levels studied, but varying less than 20% within a given rotational manifold. The error bars quoted reflect 1σ estimates based on variance/covariance matrices obtained from least squares fits to the column-integrated densities. Errors estimated in this manner are most reliable when the number of measurements is large compared to the number of parameters determined. A simple statistical analysis based on the student distribution³³ and four to six measurements for each HF(v, J) state (see Table I) predicts less than a 20% increase in these error estimations.

The HF(v, J) rotational distributions for $v=2$ and 3 are represented graphically in Fig. 5 and indicate several interesting trends. First of all, the HF(v, J) distributions at the higher collision energies appear “Boltzmann-like,” i.e., exhibiting a rapid initial growth followed by a gradual monotonic decay with increasing J . This is qualitatively similar to previous quantum state resolved observations in F+H₂ and F+CH₄ systems, and from comparison with theoretical calculations (see below), the result appears to be characteristic of *direct reactive scattering* dynamics associated with rapid H atom abstraction from the HD. Second, there is a strong dependence of cross sections on center of mass collision energy. This effect is most pronounced for the HF($v=3, J$) distributions; specifically, the peak cross sections for HF($v=3, J$) vary by over an order of magnitude for a threefold

TABLE II. Supersonic jet and collision characteristics.

v_F (m/s)	% Ar/HD	v_{HD} (m/s)	E_{perp}	E_{com}
561	0.0	2310	1.76	1.88(43)
561	3.0	1970	1.31	1.46(34)
561	9.0	1620	0.92	1.04(25)
561	25.0	1150	0.51	0.59(16)

TABLE III. HF(v, J) state-to-state relative reaction cross sections. Results are after density-to-flux transformation, scaling for dilution by argon, and division by the average collision velocity. The numbers in parentheses are 1σ errors. The cross sections have been normalized such that summing over all $E_{\text{com}} = 1.9$ kcal/mol data gives 100%.

J	$E_{\text{com}} = 1.9(4)$ kcal/mol			$E_{\text{com}} = 1.5(3)$ kcal/mol			$E_{\text{com}} = 1.0(3)$ kcal/mol		$E_{\text{com}} = 0.6(2)$ kcal/mol	
	$v=3$	$v=2$	$v=1$	$v=3$	$v=2$	$v=1$	$v=3$	$v=2$	$v=3$	$v=2$
0	2.29(10)	2.01(14)	0.59(38)	1.70(5)	1.97(11)	0.15(23)	1.01(5)	1.63(13)	0.29(4)	0.97(10)
1	4.42(15)	5.69(23)	0.72(47)	3.03(8)	4.90(15)	0.62(38)	1.42(8)	4.28(20)	0.36(7)	1.75(15)
2	3.01(13)	7.36(26)	1.32(49)	1.58(7)	6.20(20)	1.14(37)	0.86(11)	4.81(20)	0.21(7)	1.85(17)
3	1.38(13)	7.65(26)	3.01(44)	0.49(7)	6.31(22)	1.27(55)	0.39(8)	4.83(32)	0.14(8)	2.26(18)
4	0.55(15)	7.60(18)	3.21(45)	0.31(8)	6.49(13)	1.41(39)	0.25(9)	4.61(19)	-0.06(6)	1.97(18)
5	0.12(14)	7.20(28)	2.85(41)	0.12(6)	5.73(19)	1.45(30)	0.11(6)	4.47(22)	0.02(6)	1.59(16)
6	0.17(14)	5.80(27)	2.10(49)	-0.02(6)	4.27(19)	2.04(38)	-0.10(8)	3.92(17)		1.90(20)
7	0.04(14)	4.73(25)	1.75(47)		3.94(24)	1.36(35)	-0.03(4)	2.92(32)		1.48(15)
8		4.24(26)	1.15(43)		3.07(14)	1.37(39)		2.50(16)		1.34(13)
9		3.25(19)	2.11(45)		2.75(16)	0.98(34)		2.33(13)		1.86(13)
10		2.72(21)	1.07(49)		1.98(9)	1.56(31)		1.53(16)		1.27(22)
11		2.07(21)	1.26(42)		1.72(11)	0.83(27)		1.30(15)		1.22(32)
12		1.34(27)	1.58(48)		0.76(12)	1.16(27)		0.65(15)		-0.05(38)
13		0.82(70)	1.56(78)		-0.03(32)	0.68(26)		0.19(16)		0.10(45)
14		-0.28(38)	1.52(104)		0.03(22)	0.33(43)		-0.22(39)		
15		0.03(60)	-0.03(67)		0.04(11)	0.18(46)		-0.09(8)		

decrease in E_{com} . This heightened sensitivity is readily rationalized by conservation of energy constraints; the $\text{F} + \text{HD}(J=0)$ reaction is insufficiently exothermic [31.19(1) kcal/mol]^{31,32,34} to form even the lowest state in the HF($v=3, J$) manifold (32.52 kcal/mol) without the additional center of mass collision energy. In fact, a closer comparison of Figs. 3 and 5 indicates the presence of minor formation chan-

nels into 1–2 rotational levels that should be energetically closed to $\text{F}(^2P_{3/2}) + \text{HD}(J=0)$ at each E_{com} ; we will return to this point in Sec V.

By way of contrast, there is a much reduced sensitivity to collision energy in the HF($v=2, J$) manifold, which varies only by approximately equal threefold at low J for a similar threefold change in E_{com} . What is particularly noteworthy, however, is that this decreased sensitivity to E_{com} becomes quite prominent at higher J values, resulting in only modest changes in cross section at $J \approx 11$ over the same threefold range of collision energies. Stated differently, the HF($v=2, J$) distributions noticeably “flatten” with respect to J for the lowest collision energies sampled ($E_{\text{com}} \approx 0.6$ kcal/mol), as opposed to the more Boltzmann-type distributions in HF($v=2, J$) consistently observed at higher energies. From detailed calculations by Chao and Skodje,²⁰ this proves to be a characteristic product state signature for quantum transition-state resonance behavior in $\text{F} + \text{HD}$, which is theoretically predicted to occur near $E_{\text{com}} \approx 0.5\text{--}0.6$ kcal/mol.

V. DISCUSSION

The anomalous change in topology of the HF($v=2, J$) distributions with collision energy near the predicted $\text{F} + \text{HD}$ transition state resonance provides a particularly useful opportunity for benchmark comparison with full quantum wave packet calculations. The relevant data are illustrated more clearly in Figs. 6(a) and 6(b), which exhibits HF($v=2, J$) distributions at energies significantly above [$E_{\text{com}} = 1.9(4)$ kcal/mol] and essentially at [$E_{\text{com}} = 0.6(2)$ kcal/mol] the $\text{F} + \text{HD}$ transition-state resonance. Figure 6(a) indicates that the HF($v=2, J$) distributions at higher collision energies exhibit a very hot but nevertheless “thermal” looking distribution, with a slow decay in the high J tail up to 3500 cm^{-1} . Plotted also in Fig. 6(a) are results from Chao and Skodje,²⁰ where the theoretical energy dependent state-to-state cross sections have been obtained by full

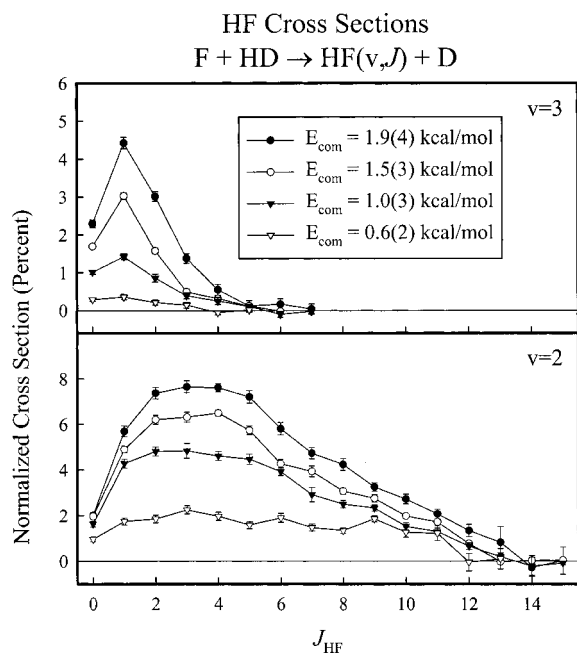


FIG. 5. HF(v, J) state-to-state reaction cross sections for $v=2, 3$ as a function of collision energy. The data are normalized such that the sum of all cross sections at 1.9 kcal/mol collision energy is 100%. A rapid decrease in $v=3$ cross sections is evident as the channel becomes energetically inaccessible. Note the much slower decrease in $v=2$ cross sections with energy, and specifically the pronounced “flattening” of the rotational distributions for collision energies [$\approx 0.6(2)$ kcal/mol] near the predicted transition state resonance.

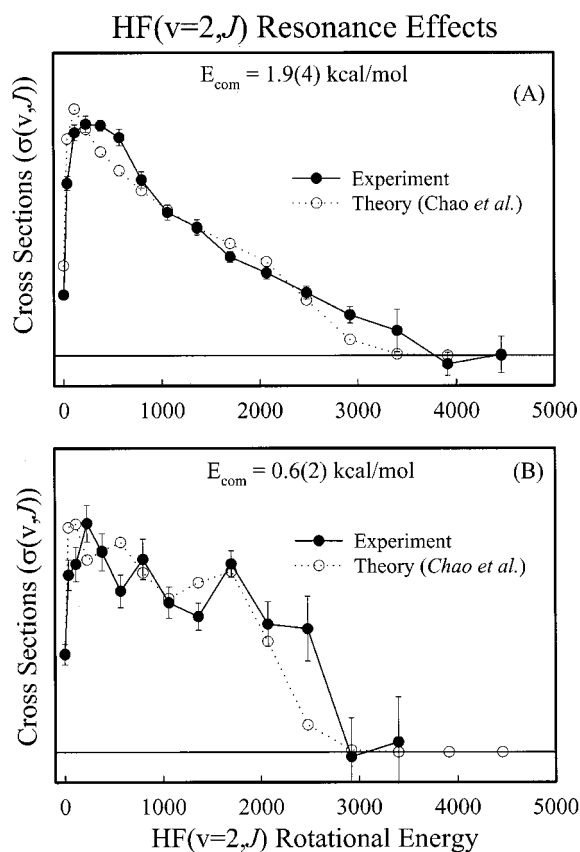


FIG. 6. Nascent HF populations for $E_{\text{com}} = 1.9(4)$ kcal/mol and $0.6(2)$ kcal/mol. Panel (A) shows typical data at higher collision energies where the dynamics are dominated by direct reactive scattering, yielding a more “Boltzmann-type” distribution which peaks at low J and gradually drops with increasing J . By way of contrast, panel (B) represents the qualitatively different J distributions obtained at energies [$E_{\text{com}} \approx 0.6(2)$ kcal/mol] near the quantum transition state resonance (Ref. 20), which are essentially “flat” in J out to $J = 11$, where they promptly drop to zero.

quantum wave packet reactive scattering on the Stark–Werner potential surface and explicitly convoluted over the measured experimental distribution in collision energies. Since the crossed-jet apparatus determines only relative state-to-state cross sections, the experimental and theoretical distributions have been normalized to both sum to unity. As clearly evident in Fig. 6(a), the agreement between experiment and theory is remarkably good. From the analysis of Chao and Skodje,²⁰ this qualitatively Boltzmann-type shape of the rotational distributions is characteristic of *direct* reactive scattering dynamics, where the reaction proceeds smoothly and rapidly “over the top” of a reaction barrier, without any quantum resonance dynamical effects due to quasibound H atom motion between the F and D atoms.

Conversely, in Fig. 6(b), the experimental distributions are shown for $HF(v=2)$ at $E_{\text{com}} = 0.6(2)$ kcal/mol, where resonance effects are theoretically predicted to be most important. The differences between *direct* reactive scattering opposed to *resonance* mediated product state distributions are immediately evident. The experimental distributions rise quickly from $J=0$ and remain relatively “flat” out to $J = 11$, where the distribution rapidly decreases to zero for $J \geq 12$. This “boxlike” type of product state distribution is

qualitatively different from all other collision systems, i.e., $F+H_2$, $F+NH_3$, and $F+CH_4$, studied thus far with the crossed jet apparatus. Plotted again for comparison in Fig. 6(b) are the theoretical results of Chao and Skodje,²⁰ convoluted over a $E_{\text{com}} = 0.6(2)$ kcal/mol collision energy distribution and normalized to unity. The theoretical curves closely recapitulate this anomalous “boxlike” dependence on the final J state; indeed, the agreement between experiment and theory is remarkably good out to the highest J values ($J \approx 11$) near 2500 cm^{-1} .

As mentioned in the introduction, the source of this anomalous, nearly “flat” distribution in J states at $E_{\text{com}} \approx 0.6$ kcal/mol has been identified by Chao and Skodje²⁰ to be tunneling dynamics out of the transition state resonance region. In essence, the tunneling escape rate from the resonance *increases* dramatically with final HF rotational state due to a combination of (i) significantly noncollinear tunneling geometries and (ii) strong lowering of the rovibrationally adiabatic tunneling barrier with asymptotic J value. The resulting balance between a J dependent *increase* in tunneling rates and J dependent *decrease* from phase-space considerations predicts a more nearly “flat” cross section distribution in J up to the energetic limit, in remarkably close agreement with experiment. This provides strong additional support from nascent quantum-state resolved populations for the existence of relatively broad quantum transition state resonances in $F+HD$ at collision energies near $E_{\text{com}} \approx 0.5\text{--}0.6$ kcal/mol, as first demonstrated in differential scattering studies by Liu and co-workers.¹⁸

Though the J state dependence of these reactive cross sections appears to be well represented, it is worth noting that some discrepancies between experiment and theory remain at the vibrational level. This can be seen in Fig. 7, where the vibrational cross sections (summed over all rotational states) are plotted against experimental results for $HF(v=2,3)$ of Liu and co-workers¹⁸ and theoretical calculations by Chao and Skodje.²⁰ For appropriate comparison with the current crossed jet results, both the experimental and theoretical data have been convoluted over the collision energy distributions previously reported in Fig. 4. Finally, since both experiments measure only relative cross sections, all three data sets have been rescaled to sum to unity. In general, the two sets of experimental results are in good agreement, each indicating threefold to fivefold higher populations in $HF(v=2)$ vs $HF(v=3)$ at collision energies above the transition state resonance, with a much steeper fractional decrease in $\sigma_{v=3}$ vs $\sigma_{v=2}$ with E_{com} . Theoretical predictions are also in qualitative agreement with experiment, though with two notable discrepancies. First of all, theory predicts a much steeper increase in reaction cross section (from 0 to 0.6 kcal/mol) for $HF(v=2)$ formation at the transition-state resonance than is observed in either experiment. Such a resonance feature is indeed confirmed in the data of Liu and co-workers,¹⁸ though the magnitude of this enhancement is considerably smaller (approximately twofold to threefold) than predicted by theory. The crossed jet data does reveal not a significant enhancement in total cross section near $E_{\text{com}} \approx 0.6$ kcal/mol, despite clear indications of resonance behavior noted above in the $HF(v=2,J)$ rotational distributions.

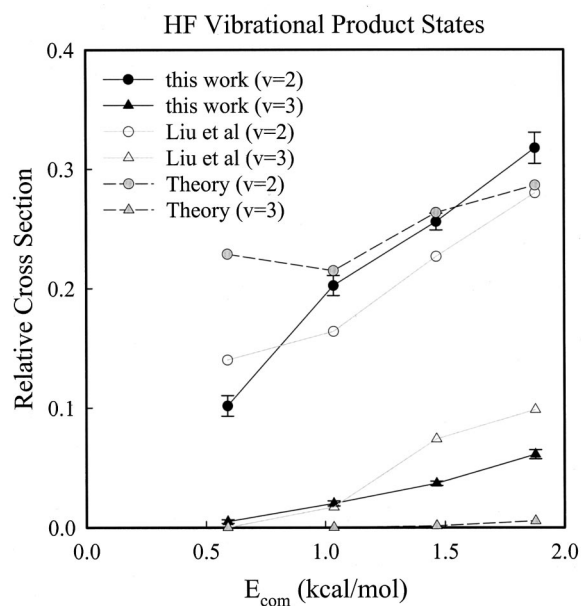


FIG. 7. Experimental and theoretical cross sections for $v=2$ and 3 at the four collision energies studied. To facilitate accurate comparison, the results of Chao and Skodje (Ref. 20) have each been convoluted over the collision energy distribution in this work, with each data set normalized to unity.

However, it is likely that this enhancement is at least partially masked by the broader energy resolution in the crossed jet configuration.

Second, the wave packet calculations substantially *underpredict* the $v=3/v=2$ branching ratios observed in both experiments by more than an order of magnitude. One reason for this discrepancy is that the HF($v=3, J$) levels are formed near the energetic limit, and governed by tunneling dynamics exponentially sensitive¹⁸ to the barrier width and height. This is relevant since the calculations were performed on the Stark and Werner potential energy surface (SW-PES³⁵). This surface does not account for the effects of spin-orbit coupling (included in HSW-PES³⁶), which adds an additional $\Delta E_{\text{spin-orbit}}/3 \approx 0.35$ kcal/mol to the SW barrier height. More relevantly near threshold, the SW potential surface underpredicts the exothermicity of the reaction by ≈ 0.38 kcal/mol, which can of course make significant differences in predicted product state distributions very close to the energetic threshold. In any event, both direct IR absorption and H atom time-of-flight experimental methods consistently yield substantially larger relative branching ratios for formation of HF($v=3$) than can be accounted for theoretically. The source of this discrepancy is currently being investigated by Chao and Skodje,²⁰ in efforts to further elucidate the specific dynamics for production into these threshold HF($v=3, J$) states.

By virtue of conservation of energy and momentum, there is a perfect *anticorrelation* between internal HF rovibrational energy and the energy released into translational recoil degrees of freedom. As a result, the observed Doppler shifts narrow substantially with increasing internal energy deposited in HF, varying by nearly 50% between HF($v''=2$, low J) [$\Delta\nu=0.017(1)$ cm^{-1}] and HF($v''=3$, low J) [$\Delta\nu=0.0111(2)$ cm^{-1}] transitions. Indeed, this competition be-

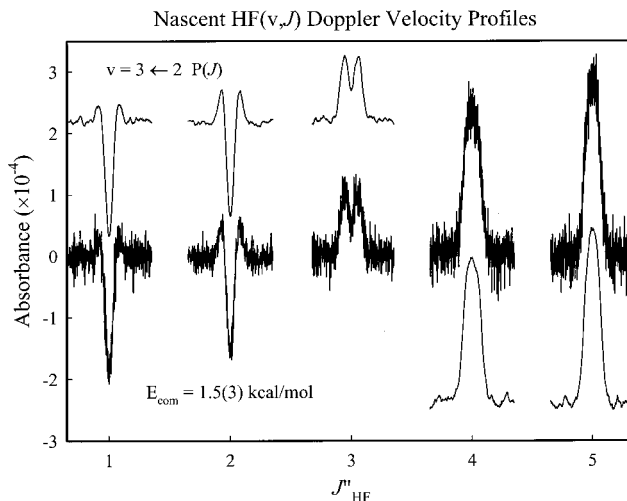


FIG. 8. High resolution HF Dopplerimetry data showing velocity dependent absorption profiles for $E_{\text{com}}=1.5(3)$ kcal/mol. By conservation of energy, the upper vibrational state populations are formed at lower recoil velocities, which preferentially lead to population inversion and thus stimulated emission near line center. These profiles also confirm the translationally unrelaxed, single collision nature of the experiments.

tween upper/lower state populations and velocity distributions can yield quite structured Doppler profiles, as shown in Fig. 8 for a series of $v'=3 \leftarrow v''=2$ P(J) transitions. Such structure arises simply from the fact that the upper state is moving more slowly than the lower state, which leads to velocity dependent population inversions and therefore stimulated emission and absorption behavior at small and large detuning from line center, respectively. This behavior has been observed previously in F+CH₄ scattering studies in this laboratory,^{21,22} where the greater mass of the CH₃ translates into much larger Doppler shifts for the recoiling HF products, permitting information on quantum state resolved nascent velocity distributions to be extracted. For the F+HD kinematics, however, the recoil energy is split much less favorably ($\approx 91\%:9\%$) between D and HF products, which for HF($v=2, J=0$) ($E_{\text{com}}=1.9$ kcal/mol) translates into recoil speeds of ≈ 650 m/s in the center-of-mass frame. For a Maxwell-Boltzmann distribution of recoil velocities, this would imply a Doppler width on the order of $\Delta\nu \approx 0.011$ cm^{-1} , which, when convoluted over experimental resolution [$\Delta\nu_{\text{FWHM}} \approx 0.0117(2)$ cm^{-1}] in the crossed jet configuration, gives 0.016 cm^{-1} and compares well with the observed Doppler structure [$0.017(1)$ cm^{-1}]. Thus, though the recoil Doppler structure is not sufficiently extensive with respect to the crossed jet resolution limit to warrant a detailed Dopplerimetry analysis, one can nevertheless demonstrate internal consistency with the data. Furthermore, the presence of such translationally unrelaxed Doppler structure confirms the rigorously single collision nature of the scattering dynamics under investigation.

As a final comment, we consider the threshold populations observed in HF($v=3, J$), which are formed near the energetic limit. The exothermicity^{31,32,34} for the F($^2P_{3/2}$) + HD($J=0$) reaction is very accurately known [$31.19(1)$ kcal/mol], which in combination with the distribution of collision energies (E_{com}), determines a rigorous upper limit on

HF(*v*,*J*) states that may be energetically populated. The inset in Fig. 3 illustrates the relevant overall reaction energetics for forming HF(*v*=3,*J*) states and the experimentally determined spread in collision energies. At $E_{\text{com}} \approx 1.9(4)$ kcal/mol, there is significant population in up to HF(*v*=3,*J*=4), which is consistent with the collision energy. As E_{com} is decreased, however, HF(*v*=3,*J*) product states continue to be formed that should be energetically inaccessible from $\text{F}(^2P_{3/2}) + \text{HD}(J=0)$ reactions. For example, HF(*v*=3,*J*=4) is clearly formed at $E_{\text{com}} = 1.5$ kcal/mol, and HF(*v*=3,*J*=3,4) are both detected at $E_{\text{com}} = 1.0(3)$ kcal/mol, despite a vanishingly small fraction of $\text{F}(^2P_{3/2}) + \text{HD}(J=0)$ collisions predicted from Fig. 4 to have sufficient energy. These discrepancies are most accentuated at $E_{\text{com}} = 0.6(2)$ kcal/mol, where no state in the *v*=3 manifold is energetically accessible; nevertheless, small but finite experimentally measured populations are clearly evident into *J*=0, 1, 2, and 3 (3 at the 2σ level). It is important to stress that this comparison is based solely on experimentally well determined asymptotic properties HF and HD, and therefore completely independent of any residual inaccuracies or approximations implicit in the *ab initio* Stark and Werner F+HD potential surface. It is also worth noting from Fig. 7 that similar results for anomalous formation of energetically inaccessible HF(*v*=3) states at low collision energies are obtained in the time of flight experiments of Liu and co-workers.¹⁸

The formation of up to *J*=3 (but not *J*=4) at $E_{\text{com}} \approx 0.6(2)$ kcal/mol necessitates an additional source of energy on the order of ≈ 1 kcal/mol. This is also consistent with previous quantum state resolved studies of F+H₂ dynamics as a function of center-of-mass collision energy, which also report nascent HF(*v*,*J*) product states ≈ 1 kcal/mol higher than can be accounted for by reaction energetics. We have carefully considered and rejected several possible sources of this additional collision energy. First of all, fractional uncertainty in the collision energy is appreciable due to angular distribution in the crossed jet configuration; however, this uncertainty scales with E_{com} and is minor (≈ 0.2 kcal/mol) under threshold collision conditions. Rationalizing these differences on the basis of “wings” in the center-of-mass collision distribution would require E_{com} out near ≈ 1.7 kcal/mol, i.e., $>5\sigma$ higher than the average value of $E_{\text{com}} \approx 0.6(2)$ kcal/mol. Another possibility would be rotationally excited HD reagent in the beam with $E_{\text{rot}} > 1$ kcal/mol. However, this would require at least HD(*J*=3), which is negligibly populated ($\ll 1\%$) at 50 K jet temperature conditions. Indeed, the present F+HD studies were specifically motivated to eliminate the ortho/para nuclear spin statistical constraints with H₂ reagent and thereby eliminate any rotational relaxation bottlenecks. A third possibility to consider would be reactions with residual H₂ in the HD jet, which by virtue of zero point energy differences could provide an additional ≈ 0.8 kcal/mol. However, the magnitude of the observed effects is simply inconsistent with H₂ impurity limits ($< 1\%$) measured experimentally, only a minor fraction of which proceeds to populate the HF(*v*=3,*J*) manifold.

The most plausible source of this internal energy is from $\text{F}^*(^2P_{1/2})$, i.e., the spin-orbit excited electronic state

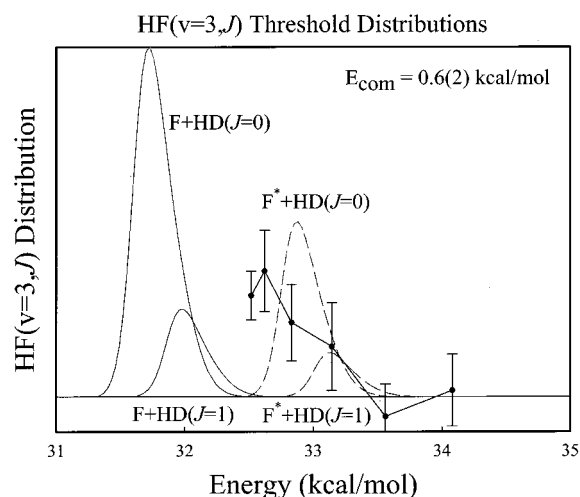


FIG. 9. Threshold HF(*v*=3) rotational distributions at $E_{\text{com}} = 0.6(2)$ kcal/mol, plotted as a function of HF(*v*,*J*) internal energy. The curves represent the distributions of total energy (i.e., $E_{\text{com}} + E_{\text{rxn}}$) available for product formation, based on HD(*J*=0,1) reaction with ground state $\text{F}(^2P_{3/2})$ atoms (solid line) or spin-orbit excited $\text{F}^*(^2P_{1/2})$ atoms (dashed line). Note that at $E_{\text{com}} = 0.6(2)$ kcal/mol there is insufficient energy to form any HF(*v*=3,*J*) levels from ground state F atom reactions, which suggests minor but finite ($< 5\%$) contributions from nonadiabatic reactions with F^* .

($\Delta E_{\text{spin-orbit}} = 1.15$ kcal/mol), which based on beam studies of Cassavecchia and co-workers³⁷ should be present in nearly statistical ($[\text{F}^*]/[\text{F}] \approx 2:4$) concentrations in the discharge expansion. Additional support for this scenario is shown in Fig. 9, which depicts the observed rotational distributions for HF(*v*=3) plotted as a function of the minimum energy required to access each quantum state. Plotted also are the distributions of energies for reactions with ground state $\text{F}(^2P_{3/2})$ and spin-orbit excited $\text{F}^*(^2P_{1/2})$ atoms, respectively, including all HD(*J*) species thermally populated in the jet. Specifically, nascent distributions in several HF(*v*=3,*J*) states inaccessible to F+HD are quite appreciable, but drop to zero (within experimental uncertainty) at the energetic limit for $\text{F}^* + \text{HD}$. By summing over the total HF(*v*,*J*) populations, the fraction of nascent product appearing in states energetically inaccessible to F+HD can be estimated to be $< 5\%$. This is quite comparable to findings previously reported for F+H₂ reactions, where equivalent discrepancies suggest the small but finite role of nonadiabatic reaction dynamics in these systems. The presence of such nonadiabatic contributions would be qualitatively consistent with the experimental results of Liu and co-workers,¹⁹ as well as high level theoretical calculations by Alexander,³⁸ which predict F^* to exhibit a small but finite reactivity at these low collision energies. Furthermore, in contrast to the major impact on product state distributions evident near threshold, the small size of these nonadiabatic effects is expected to have only minor influence for HF(*v*≤2,*J*). Indeed, this supports our use of purely nonadiabatic predictions from Chao *et al.*²⁰ for comparison between theory and experiment. It is important to note, however, that even these state-of-the-art theoretical predictions are based on F+H₂ potential surfaces that currently underpredict the experimentally known reaction exothermicity by ≈ 0.6 kcal/mol. The effect of this

surface error on near threshold theoretical predictions of state-to-state reaction dynamics is therefore of considerable concern and worthy of further investigation.

VI. SUMMARY AND CONCLUSIONS

Nascent distributions of HF quantum state distributions have been studied for the $F+HD \rightarrow HF(v,J)+D$ reaction using high-resolution direct infrared absorption in a crossed supersonic jets reaction chamber. The distributions are studied as a function of collision energy, with special attention on the results at low (0.6 kcal/mol) collision energies. These reactions, which occur just below the reaction barrier, proceed by tunneling through the barrier and go through a recently predicted¹⁸ reaction resonance. The resonance corresponds roughly to the hydrogen atom oscillating back and forth between the D and F atoms numerous times before the reaction proceeds down the product channel into $HF+D$. The recent calculations by Chao and Skodje²⁰ reveal not only unusual behavior in the angular distributions and integral cross sections, but also unusual structure in the rotational distributions of $HF(v=2)$ at low collision energies. Recent experiments by Liu and co-workers¹⁸ have yielded good agreement with the theoretically predicted integral cross sections as a function of energy, as well as revealing detailed state dependence of the differential cross sections on $HF(v)$ vibrational manifold. The thrust of the present experimental work has been toward exploiting high resolution IR detection methods to obtain fully *rovibrationally* quantum state resolved $HF(v,J)$ populations and integral cross sections. The nearly quantitative agreement between these experimental results and the theoretical resonance distributions predicted into the $HF(v=2;J)$ manifold provide strong independent confirmation for the presence of quantum transition state resonance effects in $F+HD$ reactive scattering. Furthermore, the high quantum state resolution of these studies provide additional evidence for nonadiabatic channels due to a weak but finite reactivity of F^* with HD. As we have no independent measure of the F^*/F ratio in the expansion, it is not possible to determine quantitatively the relative cross sectional contributions for F^* vs F atoms. However, at our lowest collision energies, the fraction of $HF(v,J)$ nascent product energetically inaccessible to purely adiabatic F atom reactions is <5%. This is similar to the fraction of energetically inaccessible states observed in previous $F+H_2$ studies and is also qualitatively consistent with theoretical predictions by Alexander *et al.*³⁸ for total nonadiabatic contributions to chemical reaction. However, a completely rigorous comparison between experiment and theory under such near threshold conditions for forming $HF(v=3,J)$ states will likely require potential surfaces with predictive accuracy in the reaction energetics better than the current ≈ 0.6 kcal/mol limitations.

ACKNOWLEDGMENTS

This research has been supported by funds from the Air Force Office of Scientific Research and the National Science Foundation. W. W. H. thanks the National Research Council for a postdoctoral research fellowship.

- ¹S. A. Nizkorodov, W. W. Harper, W. B. Chapman, B. W. Blackmon, and D. J. Nesbitt, *J. Chem. Phys.* **111**, 8404 (1999).
- ²W. B. Chapman, B. W. Blackmon, S. Nizkorodov, and D. J. Nesbitt, *J. Chem. Phys.* **109**, 9306 (1998).
- ³W. B. Chapman, B. W. Blackmon, and D. J. Nesbitt, *J. Chem. Phys.* **107**, 8193 (1997).
- ⁴M. Baer, M. Faubel, B. Martinez-Haya, L. Y. Rusin, U. Tappe, and J. P. Toennies, *J. Chem. Phys.* **108**, 9694 (1998).
- ⁵G. Dharmasena, K. Copeland, J. H. Young, R. A. Lasell, T. R. Phillips, G. A. Parker, and M. Keil, *J. Phys. Chem. A* **101**, 6429 (1997).
- ⁶G. Dharmasena, T. R. Phillips, K. N. Shokhirev, G. A. Parker, and M. Keil, *J. Chem. Phys.* **106**, 9950 (1997).
- ⁷M. Faubel, L. Rusin, S. Schlemmer, F. Sondermann, U. Tappe, and J. P. Toennies, *J. Chem. Phys.* **101**, 2106 (1994).
- ⁸D. M. Neumark, A. M. Wodtke, G. N. Robinson, C. C. Hayden, and Y. T. Lee, *J. Chem. Phys.* **82**, 3045 (1985).
- ⁹M. H. Alexander, H. J. Werner, and D. E. Manolopoulos, *J. Chem. Phys.* **109**, 5710 (1998).
- ¹⁰F. J. Aoiz, L. Banares, B. Martinez-Haya, J. F. Castillo, D. E. Manolopoulos, K. Stark, and H. J. Werner, *J. Phys. Chem. A* **101**, 6403 (1997).
- ¹¹J. F. Castillo, D. E. Manolopoulos, K. Stark, and H. J. Werner, *J. Chem. Phys.* **104**, 6531 (1996).
- ¹²K. Stark and H. J. Werner, *J. Chem. Phys.* **104**, 6515 (1996).
- ¹³E. Rosenman, S. Hochman-Kowal, A. Persky, and M. Baer, *Chem. Phys. Lett.* **257**, 421 (1996).
- ¹⁴J. C. Polanyi and D. C. Tardy, *J. Chem. Phys.* **51**, 5717 (1969).
- ¹⁵J. C. Polanyi and K. B. Woodall, *J. Chem. Phys.* **57**, 1 (1972).
- ¹⁶E. Wrede, L. Schnieder, K. H. Welge, F. J. Aoiz, L. Banares, J. F. Castillo, B. Martinez-Haya, and V. J. Herrero, *J. Chem. Phys.* **110**, 9971 (1999).
- ¹⁷E. Wrede and L. Schnieder, *J. Chem. Phys.* **107**, 786 (1997).
- ¹⁸R. T. Skodje, D. Skouteris, D. E. Manolopoulos, S. H. Lee, F. Dong, and K. Liu, *J. Chem. Phys.* **112**, 4536 (2000).
- ¹⁹F. Dong, S. H. Lee, and K. Liu, *J. Chem. Phys.* **113**, 3633 (2000).
- ²⁰S. Chao and R. T. Skodje (private communication).
- ²¹W. W. Harper, S. A. Nizkorodov, and D. J. Nesbitt, *J. Chem. Phys.* **113**, 3670 (2000).
- ²²W. W. Harper, S. A. Nizkorodov, and D. J. Nesbitt, *Chem. Phys. Lett.* **335**, 381 (2001).
- ²³This is a trade name used for identification purposes only and does not constitute an endorsement by the authors or their institutions.
- ²⁴D. Proch and T. Trickl, *Rev. Sci. Instrum.* **60**, 713 (1989).
- ²⁵D. D. Nelson, Jr., A. Schifman, K. R. Lykke, and D. J. Nesbitt, *Chem. Phys. Lett.* **153**, 105 (1988).
- ²⁶D. Herriott, H. Kogelnik, and R. Kompfner, *Appl. Opt.* **3**, 523 (1964).
- ²⁷D. Kaur, A. M. Souza, J. Wanna, S. A. Hammad, L. Mercorelli, and D. S. Perry, *Appl. Opt.* **29**, 119 (1990).
- ²⁸A. Savitzky and M. J. E. Golay, *Anal. Chem.* **36**, 1627 (1964).
- ²⁹E. Arunan, D. W. Setser, and J. F. Ogilvie, *J. Chem. Phys.* **97**, 1734 (1992).
- ³⁰W. T. Zemke, W. C. Stwalley, S. R. Langhoff, G. L. Valderrama, and M. J. Berry, *J. Chem. Phys.* **95**, 7846 (1991).
- ³¹W. C. Stwalley, *Chem. Phys. Lett.* **6**, 241 (1970).
- ³²W. T. Zemke, W. C. Stwalley, J. A. Coxon, and P. G. Hajigeorgiou, *Chem. Phys. Lett.* **177**, 412 (1991).
- ³³*Handbook of Mathematical Functions*, edited by M. Abramowitz and I. A. Stegun, National Bureau of Standards Applied Mathematics Series 55 (NBS, Washington, DC, 1964).
- ³⁴G. Herzberg, *Molecular Spectra and Molecular Structure I. Spectra of Diatomic Molecules* (Van Nostrand, New York, 1945), pp. 532–533.
- ³⁵D. E. Manolopoulos, *J. Chem. Soc., Faraday Trans.* **93**, 673 (1997).
- ³⁶J. F. Castillo, B. Hertke, H. J. Werner, F. J. Aoiz, L. Banares, and B. Martinez-Haya, *J. Chem. Phys.* **109**, 7224 (1998).
- ³⁷M. Alagia, V. Aquilanti, D. Ascenzi, N. Balucani, D. Cappelletti, L. Cartechini, P. Cassavechia, F. Pirani, G. Sanchini, and G. G. Volpi, *Isr. J. Chem.* **37**, 329 (1997).
- ³⁸M. H. Alexander, D. E. Manolopoulos, and H. J. Werner, *J. Chem. Phys.* **113**, 11084 (2000).